Tellus (1993), 45A, 299–310
Printed in Belgium – all rights reserved

TELLUS
ISSN 0280–6495

Generation of ringlets

By DORON NOF, *Department of Oceanography B-169 and the Geophysical Fluid Dynamics Institute, The Florida State University, Tallahassee, Florida 32306-3048, USA*

(Manuscript received 27 November 1992; in final form 6 April 1993)

ABSTRACT

A mechanism for the generation of ringlets (i.e., small cyclonic eddies (20–40 km) which have recently been observed on the periphery of warm-core rings) is proposed. The suggested process is examined analytically using a reduced gravity one-and-a-half-layer and two-and-a-half-layer model. The underlying hypothesis is that the ringlets are formed by the expulsion of fluid from the outer rim of the warm ring and that this expulsion is the result of an absorption of foreign water into the core of the ring. This nonlinear process is examined using the not-so-frequently used integrated angular momentum constraint as well as the familiar conservation of potential vorticity and mass. These constraints show that when the ring interacts with other bodies of water such as shelf water or the Gulf Stream, the shelf water is sucked into the ring in such a manner that the entire ring is capped. To conserve angular momentum, some other fluid must then be pushed out and it is argued that via instability of the ring's edge, this expulsion forms ringlets.

1. Introduction

Both satellite images and direct oceanic observations have recently demonstrated that relatively small ($\sim$10–40 km) cyclonic eddies are frequently present near the periphery of warm-core rings (see Fig. 1 and Kennelly et al., 1985). These ringlets (eddies) typically have an orbital speed of 40 cm s^{-1}, a depth of 1000 meters or so and a lifetime of a few weeks. The question of how such ringlets are formed is important because of its direct relevance to the distribution of energy, momentum and heat within the mesoscale. It is believed that this question can be, at least partially, answered by considering simplified models.

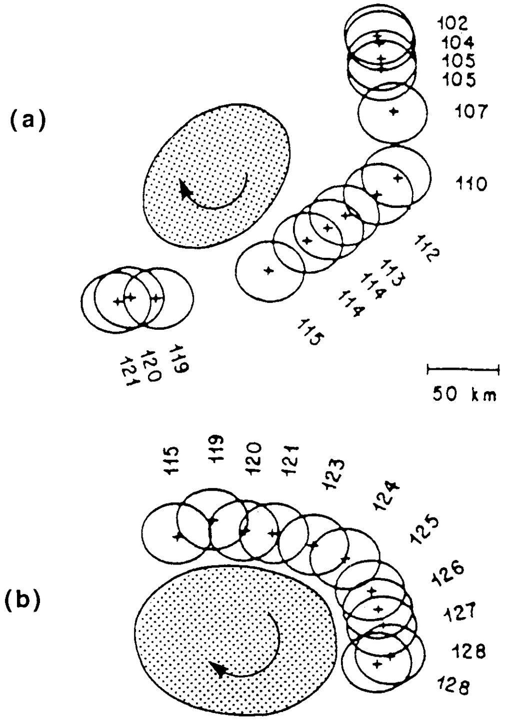

Fig. 1. (a) Cartoon derived from successive satellite images showing a ringlet around warm-core ring (WCR) 82B from day 102 to day 121. (b) This cartoon shows a ringlet around WCR 82B from day 115 to day 128. The angular momentum associated with the slow anticyclonic drift displayed in the figure is rather small compared to the angular momentum associated with the position of the ringlets and will be, therefore, neglected in our computations. Adapted from Kennelly et al. (1985).

With this idea in mind, two nonlinear inviscid models will be considered in detail. The first is a nonlinear two-and-a-half-layer model (Section 2) consisting of a zero potential vorticity warm-core ring and a one-dimensional uniform potential vorticity current (with a different density) situated several deformation radii away (Figs. 2–5). The slightly lighter one-dimensional current represents either the shelf water (which is lighter due to its lower salinity) or the Gulf Stream (which is lighter due to its higher temperature). As satellite images suggest, the ring interacts with the current and, as a result, the ring absorbs some of the lighter fluid from the edge of the current (see, e.g., images of ring 81B presented by Evans et al., 1985).

The time-dependent absorption process will not be modeled in detail but the states prior to and after the absorption will be connected with the aid of known integrated constraints. We shall see that an analytical solution of the local equations of motion indicates that the absorbed lighter fluid cannot be present in the core alone. Instead, it must spread over the entire ring until the ring is completely capped (Fig. 4). Assuming that the amount of water absorbed by the ring is small, the (not so frequently used) integrated angular momentum principle will then be applied to illustrate analytically that, since the light (current) water has been brought closer to the ring's center from its original pre-interaction position, some other fluid must be pushed out. The expulsion of ring fluid takes place in terms of instability resulting in satellite eddies (or ringlets). These ringlets cause an increase in angular momentum which compensates for the decrease of angular

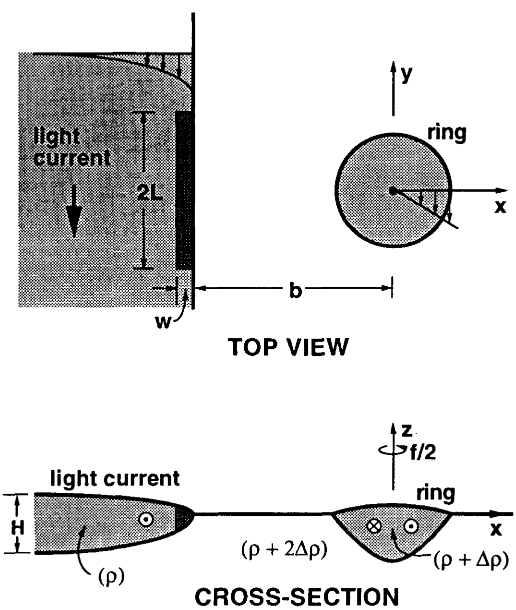

Fig. 2. Schematic diagram of the conditions prior to the interaction of a zero-potential vorticity ring with a finite potential vorticity current. The densely shaded area of the one-dimensional current will later be absorbed by the ring which, in turn, will expel fluid in the form of satellite eddies (Figs. 3, 4).

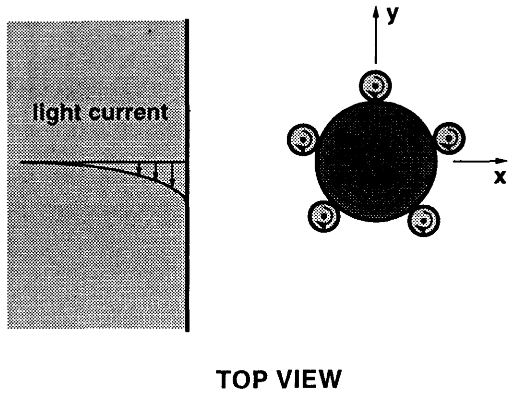

Fig. 3. The final after-interaction state corresponding to a zero potential vorticity ring. The ring is entirely capped by the light current water and anticyclonic ringlets which have been ejected from the parent ring are now present near the edge.

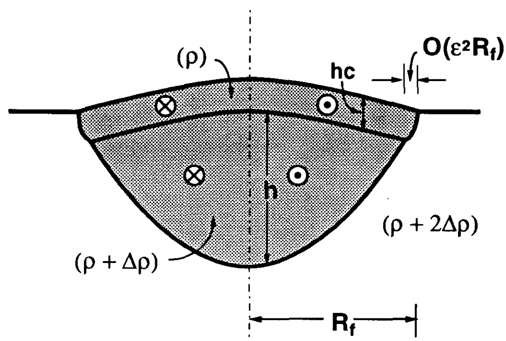

Fig. 4. Schematic diagram of the capped ring. The detailed solution shows that the entire ring must be covered by the light fluid (density ρ) absorbed from the current (see text). R_f is the final radius of the ring, h_c is the cap depth, h the depth of the ring and ε is the ratio of the initial strip width w (see Fig. 2) to the deformation radius, $(g'H)^{1/2}/f$.

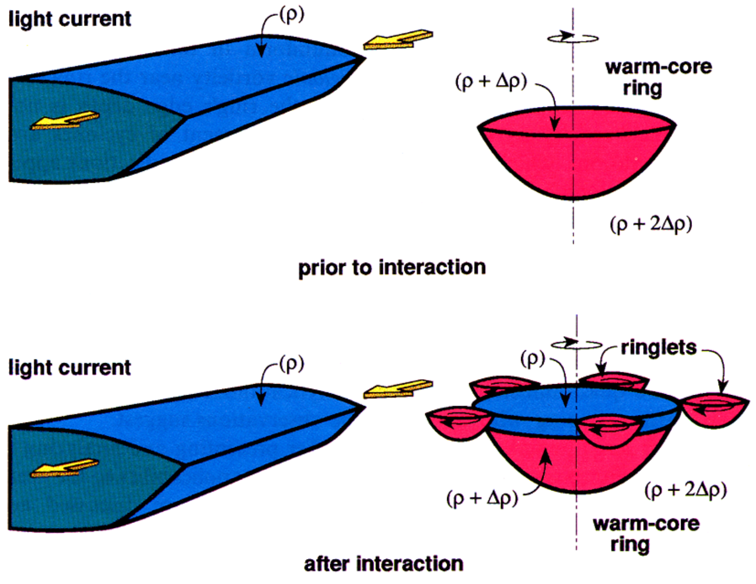

Fig. 5. A three-dimensional view of the interactions shown in Figs. 2, 3. Water from the light current (whose density is ρ) floods and caps the ring (whose density is $(\rho + \Delta\rho)$) which, in turn, ejects small anticyclones (ringlets).

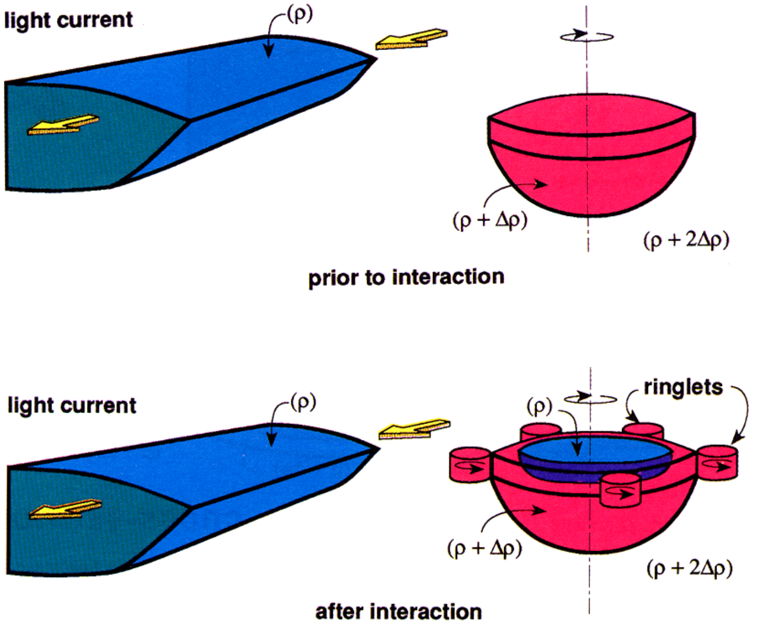

Fig. 6. A three-dimensional view of the two-and-a-half-layer model. As before, water from the light current floods the slightly heavier ring which, in turn, expels fluid to the surroundings. However, in contrast to the previous one-and-a-half-layer model (Fig. 4), the warm ring has cyclonic vorticity around the edge and the depth is finite along the rim. Consequently, the expelled fluid forms *cyclones* rather than anticyclones.

momentum associated with the absorbed light fluid drawn into the ring.

Since the anticyclonic vorticity of the ring in this particular analytical model is uniform, the satellite eddies have anticyclonic vorticity as well. This contradicts actual observations which point to cyclonic, rather than anticyclonic, satellite eddies. Obviously, the discrepancy results from the fact that actual rings do not have uniform vorticity as the model assumes. Instead, the actual vorticity of warm-core rings is usually anticyclonic in the core and *cyclonic* near the edge. Hence, the above discrepancy can be resolved by considering a more complicated and realistic quasi-numerical model which examines a warm-core ring with a finite nonuniform (rather than zero) potential vorticity (Section 3). The general approach used in this two-and-a-half-layer quasi-numerical model (Fig. 6) is the same as in the previous analytical model, i.e., the states prior to and after the interaction are connected using the integrated angular momentum principle.

However, since the ring's potential vorticity is nonuniform in this case, it allows for realistic *cyclonic* vorticity near the ring's edge (Figs. 6–8). Also, the ring's edge depth is nonzero allowing the establishment of cyclones around the edge. Although these modifications appear to be minor, they make the problem analytically intractable. Consequently, the equations of motion for both the initial and final states, as well as the connecting equations, are solved numerically. As expected, the results show that, again, an expulsion of fluid must take place and that, consequently, ringlets are formed. However, in contrast to the previous analytical model, the ringlets are now cyclonic as the observations suggest.

After presenting and analyzing these models in detail, their applicability to the ocean is considered and the results are discussed and summarized (Section 4). Because of the various states being considered, the notation and definition of variables

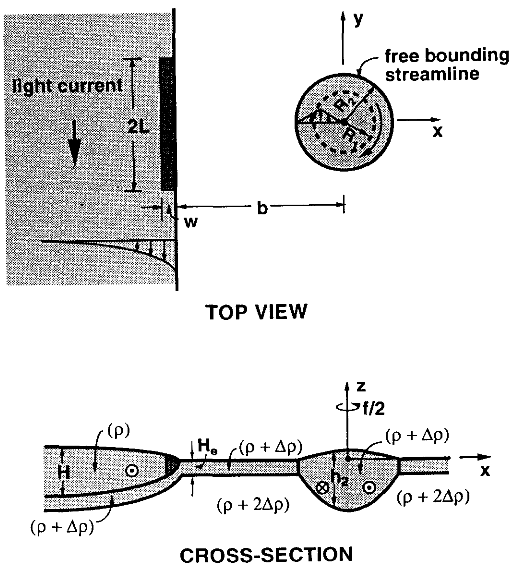

Fig. 7. Details of the two-and-a-half-layer model shown schematically in Fig. 6. The ring now has a finite nonuniform potential vorticity corresponding to a velocity profile with an anticyclonic vorticity in the core ($r \leqslant R_1$), cyclonic vorticity along the rim ($R_1 \leqslant r \leqslant R_2$) and vanishing velocity along the edge. Also, in contrast to the one-and-a-half-layer case shown in Fig. 2, the depth along the edge (H_e) is nonzero.

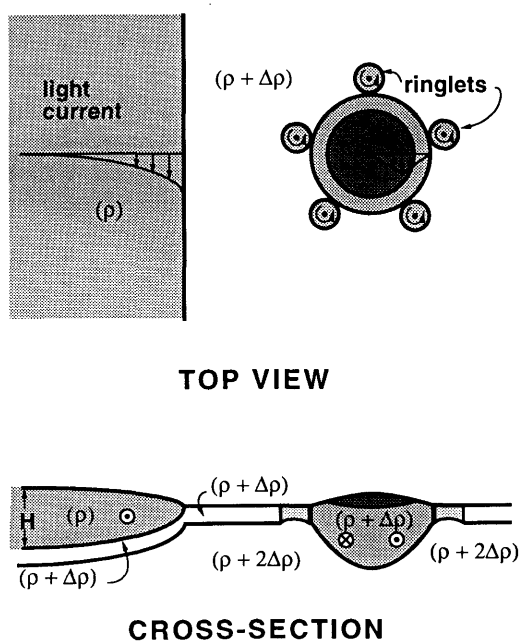

Fig. 8. The final after-interaction state corresponding to a finite nonuniform potential vorticity ring (Fig. 7). In contrast to the zero potential vorticity case (one-and-a-half-layer model) where the ring is entirely capped by the absorbed fluid, the ring is now only partially capped (densely shaded area) with the light current water. Cyclonic ringlets which have been ejected from the rim of the parent ring are present near the edge.

in unavoidably cumbersome. To ease this burden, all variables are defined in both the text and an appendix.

2. Analytical model of a zero-potential vorticity ring

Consider again the model shown in Figs. 2–5. Recall that the ring-current collision and the resulting interaction will not be examined in detail because these processes are both time-dependent and highly nonlinear making analytical tractability virtually impossible. Instead, we shall connect the final and initial states using various integrated constraints. Although this approach is not useful with regard to the time-dependent processes themselves, it provides crucial information about the end result of the interaction. The method is not new; it has been used successfully before in various studies, the most closely related being those of Nof (1990a, 1991). In polar coordinates (r, θ), the initial conditions for the zero potential vorticity ring are:

$$v_\theta = -\tfrac{1}{2} fr, \qquad h = \hat{h} - f^2 r^2/8g', \tag{2.1}$$

where $\hat{h}$ is the depth at the ring's center and the remaining notation is conventional (i.e., v_θ is the orbital speed, g' the "reduced gravity" and f is the Coriolis parameter). Similarly, the initial light current is described by,

$$v = \sqrt{2g'H}\, \mathrm{e}^{-(x-b)/\sqrt{2}R_\mathrm{d}}, \qquad h = H(1 - \mathrm{e}^{-(x-b)/\sqrt{2}R_\mathrm{d}}), \tag{2.2}$$

where the coordinate system is now Cartesian (x, y), H is the undisturbed current depth at infinity $(x \to \infty)$, b the distance between the strip and the ring (Fig. 7), and R_d is the Rossby radius $(g'H)^{1/2}/f$.

2.1. General constraints

In addition to the familiar conservation of potential vorticity and volume, the following (not so familiar) constraints connect the initial and final states.

(i) *Conservation of momentum and the center of mass.* It is a simple matter to show using the shallow water equations that, for a patch whose depth vanishes along the rim (Ball 1963, Nof 1990a) the following integrals must be satisfied:

$$\frac{\mathrm{d}}{\mathrm{d}t}\iint h(u - fy)\,\mathrm{d}x\,\mathrm{d}y = \frac{\mathrm{d}}{\mathrm{d}t}\iint h(v + fx)\,\mathrm{d}x\,\mathrm{d}y = 0. \tag{2.3}$$

Again, the (Cartesian) notation is conventional (i.e., u and v are the speeds) and the integrals are taken over the whole patch. Since in both the (steady) initial and final states the streamfunction ψ (defined by $\partial\psi/\partial x = vh$; $\partial\psi/\partial y = -uh$) is a constant along the edge, it follows from (2.3) that,

$$\frac{\mathrm{d}}{\mathrm{d}t}\iint hy\,\mathrm{d}x\,\mathrm{d}y = \frac{\mathrm{d}}{\mathrm{d}t}\iint hx\,\mathrm{d}x\,\mathrm{d}y = 0,$$

which implies that the final center of gravity must coincide with the initial center of mass.

(ii) *Torque.* The conservation of integrated angular momentum for a patch whose depth vanishes along the rim is discussed by Ball (1963), Cushman-Roisin (1989) and Nof (1990a, b, 1991). Its most general form is,

$$\frac{\mathrm{d}}{\mathrm{d}t}\iint_\mathrm{S} h[xv - yu + f(x^2 + y^2)/2]\,\mathrm{d}x\,\mathrm{d}y = 0, \tag{2.4a}$$

where the integration is done over the entire area. In polar coordinates (r, θ), it is given by

$$\frac{\mathrm{d}}{\mathrm{d}t}\iint (fr^2/2 + rv_\theta)\,hr\,\mathrm{d}r\,\mathrm{d}\theta = 0, \tag{2.4b}$$

where, as before, v_θ is the orbital velocity. In this context, it is worth pointing out that the angular momentum (AM) of a circular vortex situated a distance r_0 away from the center of the system is,

$$\mathrm{AM} = \iint_\mathrm{S} [\tfrac{1}{2} fr_0^2 + \tfrac{1}{2} fr^2 + rv_\theta]\, h\,\mathrm{d}r\,\mathrm{d}\theta,$$

where r and v_θ are now measured relative to the eddy's own center.

2.2. Scaling

To connect the initial and final state a perturbation expansion in ε, the ratio between the width of the strip (which will later be absorbed by the ring) and the deformation radius, will be used. This expansion essentially implies that the light water absorbed by the ring originates from a narrow strip along the edge of the current (Fig. 2) and that the entrained amount is small compared to the volume of the ring. The relevant nondimensional variables and scales are,

$$v_\theta^* = v_0/(g'H)^{1/2}, \qquad h^* = h/H,$$
$$R_d = (g'H)^{1/2}/f, \qquad \varepsilon^{1/2} \equiv w/R_d,$$
$$(\hat{h})^* = \hat{h}/H, \qquad h_c^* = h_c/\varepsilon H,$$
$$b^* = b/R_d, \qquad L^* = L/R_d,$$
$$r^* = r/R_d, \tag{2.5}$$

where h_c is the depth of the cap (Fig. 4), w and L are the width and length of the strip, b the strip's distance from the ring, and, as mentioned earlier, $\hat{h}$ is the ring's central depth ($\sim O(H)$).

2.3. *The capped ring*

The equations governing the final ring and the absorbed fluid above (Fig. 5) are,

$$v_{\theta c}^2/r + f v_{\theta c} = g' \frac{\partial h}{\partial r} + 2g' \frac{\partial h_c}{\partial r}, \tag{2.6}$$

$$v_\theta^2/r + f v_\theta = g' \left(\frac{\partial h}{\partial r} + \frac{\partial h_c}{\partial r} \right), \tag{2.7}$$

$$\frac{\partial v_\theta c}{\partial r} + \frac{v_{\theta c}}{r} + f = f h_c/H, \tag{2.8}$$

$$\frac{\partial v_\theta}{\partial r} + \frac{v_\theta}{r} + f = 0, \tag{2.9}$$

where terms without a subscript correspond to the ring and the subscripted "c" indicates association with the cap. The boundary conditions are: (i) the orbital speed vanishes at the center ($v_\theta^* = 0$; $r^* = 0$), (ii) both the ring's depth h and the cap's depth h_c must vanish at a finite distance from the center. Since the solution of (2.9) is $v_\theta = -\frac{1}{2} f r$, eqs. (2.6), (2.7) and (2.8) can be combined to give,

$$\frac{(v_{\theta c}^*)^2}{r^*} + v_{\theta c}^* = -\frac{1}{4} r^* + 2\varepsilon \frac{\partial h_c^*}{\partial r^*}, \tag{2.10}$$

$$\frac{\partial v_{\theta c}^*}{\partial r^*} + \frac{v_{\theta c}^*}{r^*} + 1 = \varepsilon h_c^*, \tag{2.11}$$

where the nondimensional variables introduced in (2.5) have been used.

We now expand $v_{\theta c}^*$ and hc^* in powers of ε,

$$v_{\theta c}^* = v_c^{(0)} + \varepsilon v_c^{(1)} + \cdots,$$
$$h_c^* = h_c^{(0)} + \varepsilon h_c^{(1)} + \cdots,$$

and substitute into (2.10–2.11). The zeroth (ε^0) and first (ε^1) order balances are,

$$\frac{(v_c^{(0)})^2}{r^*} + v_c^{(0)} = -\frac{1}{4} r^*, \tag{2.12a}$$

$$\frac{\partial v_c^{(0)}}{\partial r^*} + \frac{v_c^{(0)}}{r^*} + 1 = 0, \tag{2.12b}$$

$$\frac{2 v_c^{(0)} v_c^{(1)}}{r^*} + v_c^{(1)} = \frac{2\, \partial h_c^{(0)}}{\partial r^*}, \tag{2.13a}$$

$$\frac{\partial v_c^{(1)}}{\partial r^*} + \frac{v_c^{(1)}}{r^*} = h_c^{(0)}. \tag{2.13b}$$

The solution of (2.12) is,

$$v_c^{(0)} = -\tfrac{1}{2} r^*, \tag{2.14}$$

which together with (2.13a) gives,

$$h_c^{(0)} = \text{constant} = (h_c)^*, \tag{2.15}$$

indicating that the cap must extend all over the ring.

Substitution of (2.15) into (2.13b) gives

$$v_c^{(1)} = \tfrac{1}{2} (h_c)^* \, r^*$$

so that the total solution is,

$$v_c^* = -\tfrac{1}{2} r^* + \varepsilon (h_c)^* \, \tfrac{1}{2} r^* + \cdots \tag{2.16a}$$

$$h_c^* = (h_c)^* + O(\varepsilon) + \cdots \tag{2.16b}$$

where, due to our particular scaling, the absolute value of the neglected terms is of $O(\varepsilon^4)$ in both (2.16a) and (2.16b).

It is possible to show that the edge of the cap (i.e., the part of the cap that hangs out and is in direct contact with the lower layer as shown in Fig. 4) has a width of $O(\varepsilon R_d)$. It will become clear later that, due to this small width, the edge's contribution to the momentum and volume balances is negligible. Consequently, the detailed solution of the edge is not presented.

2.4. Connecting the final and initial states

By equating the volume of the light strip to the cap's volume, one finds,

$$L^*/\sqrt{2} = \pi (R_i^*)^2 (h_c)^* + O(\varepsilon), \qquad (2.17)$$

where R_i^* is the initial radius of the ring. Similarly, conservation of volume for the slightly heavier ring and ringlets gives,

$$(R_i^*)^2 \hat{h}^{(1)} = (R_i^*)^2 (h_c)^* - 4N[(\hat{h}_r)^*]^2 + O(\varepsilon), \qquad (2.18)$$

where, as mentioned, $\hat{h}^{(1)}$ is the nondimensional perturbation to the ring's original central depth $(\hat{h})^*$, $(\hat{h}_r)^*$ is the nondimensional ringlet's central depth, and N is the number of ringlets.

Conservation of total angular momentum gives,

$$L^*[b^*(b^* + 2^{3/2}) + (L^*)^2/3] = 2^{5/2}\pi N (R_i^*)^2 [(\hat{h}_r)^*]^2 + O(\varepsilon), \qquad (2.19)$$

which, as we shall shortly see, is the most informative constraint. (Note that the angular momentum of the cap and the cap's edge are $O(\varepsilon^2)$ and $O(\varepsilon^3)$, respectively, so that both are negligible; also, the volume of the cap's edge is negligible.) The solution (2.17), (2.18), and (2.19) gives the three unknowns, the uniform nondimensional cap's depth $(h_c)^*$, the nondimensional change in the ring's central depth $\hat{h}^{(1)}$, and the ringlets' central depth $(\hat{h}_r)^*$ as a function of the four known variables, the nondimensional length of the initial strip L^*, its distance from the ring b^*, the number of ringlets N, and the original radius of the ring R_i^*. It is straightforward to show that, to the order of approximation being considered, there is no change in the position of the system's center of gravity, i.e., constraint (2.3) is satisfied as should be the case.

Relation (2.19) clearly illustrates that the *angular momentum cannot be conserved without an ejection of ringlets* (i.e., N can never be zero). Since the ringlets are probably formed by instability along the edge, their most likely number is determined by the wave number of the most unstable mode. Paldor and Nof (1990) have shown that mode number five is the most unstable one for a lens and we shall, therefore, consider $N = 5$. This number of ringlets is consistent with actual observations which demonstrate that, at each given time, as many as 6 ringlets are present along the periphery (Kennelly et al., 1985).

For 5 ringlets and an initial light strip (with a total length of two deformation radii ($L^* = 1$) and a width of a third of a deformation radius ($\varepsilon^{1/2} = 1/3$)) situated 3 deformation radii away ($b^* = 3$) from a ring with an initial central depth identical to the current depth at infinity, one finds a ringlet's central depth which is about 1.8% of the parent ring's depth. The corresponding cap's depth is roughly 0.3% of the parent ring's initial depth and the decrease in the initial (parent) ring's central depth is about 0.4%.

It is a simple matter to compute the energy loss associated with the ring-current interaction. One finds that, to the order of approximation being used, the energy of the ringlets is negligible and that the energy loss (ΔE) is,

$$\Delta E = \varepsilon\{[b^*(b^* + 2^{3/2}) + (L^*)^2/3]/16\sqrt{2} + \pi L^*/\sqrt{2}\}, \qquad (2.20)$$

which is always positive as should be the case. For the numerical example previously discussed, the energy loss is 34%.

Before proceeding to the numerical computations, it should be pointed out that, in the above example, the ringlets are rather small compared to the parent ring (a few %). This results from our perturbation expansion and is not consistent with the observations which suggest a ringlets size of about a quarter or so of the parent ring (Kennelly et al., 1985). We shall see shortly that this discrepancy is resolved with the numerical computations where the ringlet's size can be as much as 20% of the parent ring.

3. Numerical computations for a varying potential vorticity ring with a finite depth along the rim

Consider again the situation shown in Figs. 6–8. As mentioned, in contrast to the zero potential vorticity case where the ring's vorticity is uniform, the ring's vorticity is now anticyclonic in the center but cyclonic around the rim. Also, the depth around the edge is now finite (rather than zero) so that an expulsion of fluid from the edge is going to form cyclones rather than anticyclones. This is not only more realistic in terms of the velocity and depth fields but, as expected, it is also more in line with the observations which show that the ringlets are cyclonic rather than anticyclonic.

The principles of the computations are the same as before except that, due to their complexity, they are carried out numerically. Because of the finite depth along the rim, it is now technically possible to lose angular momentum to the exterior fluid surrounding the ring. Using a rigorous not-so-trivial scaling analysis, Nof (1990b) has shown, however, that, if the process in question is slow compared to the ring's orbital speed, the loss of angular momentum to the surrounding fluid is negligible. Furthermore, Nof's (1990b) analysis showed that the leakage of torque through the boundary of the vorticity patch is so small that, even though it is active over a long period of time, it is still negligible. It is reasonable to assume that, as in other eddy interaction processes, the process in question is also slow and, therefore, the loss of angular momentum is ignored.

In addition to the constraints mentioned earlier, the interior of the parent ring as well as the ringlets must, of course, satisfy that potential vorticity and momentum equations. The ring's initial state is associated with the equations,

$$\frac{1}{r}\frac{\mathrm{d}}{\mathrm{d}r}(rv_\theta)+f=h\frac{f}{H_{\mathrm{p1}}}, \qquad 0\leqslant r\leqslant R_1, \tag{3.1}$$

$$\frac{1}{r}\frac{\mathrm{d}}{\mathrm{d}r}(rv_\theta)+f=h\frac{f}{H_{\mathrm{p2}}}, \qquad R_1\leqslant r\leqslant R_2, \tag{3.2}$$

$$\frac{v_\theta^2}{r}+fv_\theta=g'\frac{\mathrm{d}h}{\mathrm{d}r}, \qquad 0\leqslant r\leqslant R_2, \tag{3.3}$$

which are subject to the following boundary and matching conditions,

$$v_\theta=0, \qquad r=0, \qquad r=R_2, \tag{3.4}$$

$$h=\hat{h}, \qquad r=0, \tag{3.5}$$

$$h=H_{\mathrm{e}}, \qquad r=R_2, \tag{3.6}$$

$$v_\theta|_{r=R_1-\mu}=v_\theta|_{r=R_1+\mu}, \qquad \mu\to 0. \tag{3.7}$$

Here, H_{p1} and H_{p2} are the potential vorticity depths of the core ($r\leqslant R_1$) and rim ($R_1\leqslant r\leqslant R_2$), and μ is a small parameter. Conditions (3.4) represent the vanishing of the orbital speed at the center and along the outer edge (i.e., the velocities of the parent ring are continuous everywhere), (3.5) and (3.6) reflect the conditions that at the center and edge the depths are $\hat{h}$ and H_{e}, and (3.7) states that the velocity matches along the potential vorticity front ($r=R_1$). Given the radii R_1, R_2 and the matched orbital speed along the front, the set (3.1)–(3.3) is solved numerically for the ring's central depth $\hat{h}$, and the potential vorticity depths H_{p1} and H_{p2}. This was done by integrating outward from the center using a Runge–Kutta solver from the Numerical Recipes Software Package (Press et al., 1986).

For the two-layered final state the modified governing equations are,

$$v_{\theta\mathrm{c}}^2/r+fv_{\theta\mathrm{c}}-(v_\theta^2/r+fv_\theta)=g'\frac{\mathrm{d}h_{\mathrm{c}}}{\mathrm{d}r}, \tag{3.8}$$

$$v_\theta^2/r+fv_\theta=g'\left(\frac{\mathrm{d}h}{\mathrm{d}r}+\frac{\mathrm{d}h_{\mathrm{c}}}{\mathrm{d}r}\right), \tag{3.9}$$

$$\frac{\mathrm{d}v_{\theta\mathrm{c}}}{\mathrm{d}r}+\frac{v_{\theta\mathrm{c}}}{r}+f=f\frac{h_{\mathrm{c}}}{H}, \tag{3.10}$$

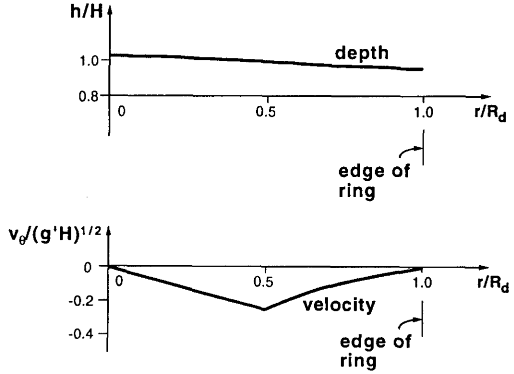

Fig. 9. The initial depth (upper panel) and velocity (lower panel) of the parent ring used in the numerical experiment. The nondimensional potential vorticity depths of the core and rim are about 65 and 0.075 (respectively) so that the core is as close to a state of zero potential vorticity as the numerical scheme allows. The corresponding initial conditions of the strip, which is later entrained by the ring, are as follows: The nondimensional width is 0.1, the length and distance from the ring center are both 2 deformation radii. The depth of the stagnant fluid surrounding the ring is identical to the current's undisturbed depth. The edge of the ring is located at $r=(g'H)^{1/2}/f$.

$$\frac{dv_\theta}{dr}+\frac{v_\theta}{r}+f=\frac{h}{H_{p1}}, \qquad 0<r\leqslant R_1, \tag{3.11}$$

$$\frac{dv_\theta}{dr}+\frac{v_\theta}{r}+f=f\frac{h}{H_{p2}}, \qquad R_1<r\leqslant R_2. \tag{3.12}$$

where, as before, the subscript "c" indicates association with the cap and no subscript indicates association with the ring.

As we shall shortly see, the boundary and matching conditions are essentially the same as before except that they need to be applied in different locations. There are a total of 7 unknowns: the cap, ring and ringlets' central depths, the new radii of the ring core (R_1) and the rim (R_2), the radius of the cap and the radius of the ringlets.

The governing equations are now integrated numerically using Runge–Kutta and the following 7 conditions are imposed:

(1) the cap's edge depth vanishes;

(2) the ring's edge depth equals H_e;

(3) the ringlet's edge depth equals H_e;

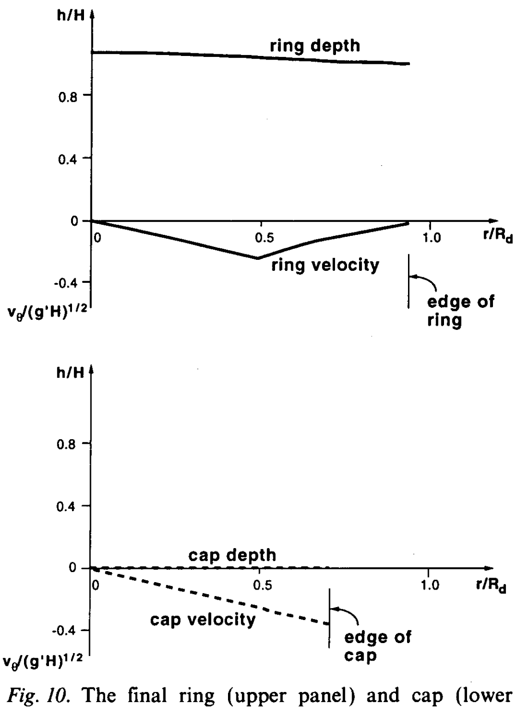

Fig. 10. The final ring (upper panel) and cap (lower panel) depth and velocity profiles corresponding to the numerical experiments. Solid lines correspond to the ring and dashed lines correspond to the cap.

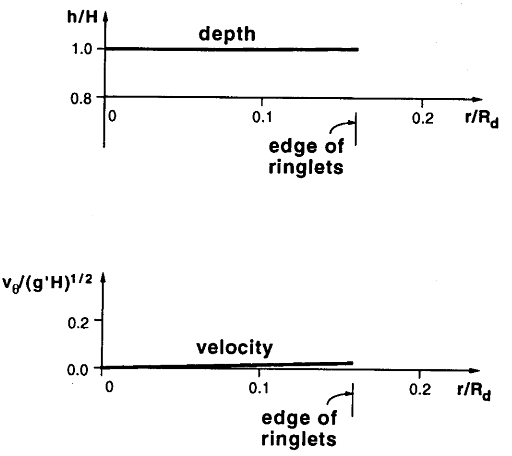

Fig. 11. The ringlets' depth and velocity profiles.

(4) conservation of the ring's core volume ($r\leqslant R_1$);

(5) conservation of the ring's rim volume ($R_1\leqslant r\leqslant R_2$);

(6) conservation of strip and cap volume;

(7) conservation of total angular momentum.

The solution for the 7 resulting equations is also found numerically. The results of 2 "typical" numerical experiments are shown in Figs. 9–14.

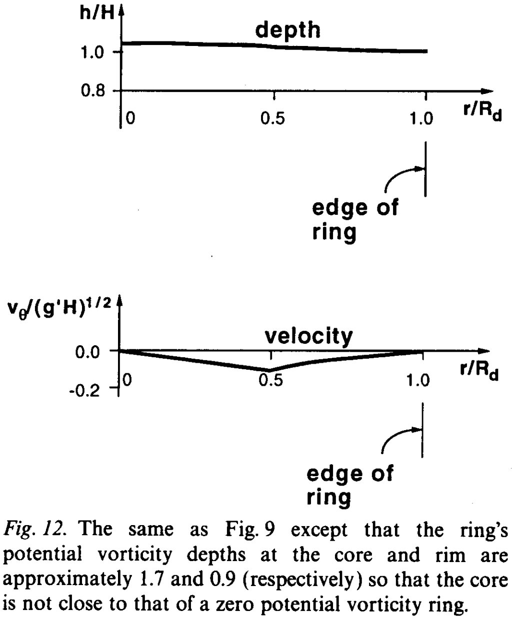

Fig. 12. The same as Fig. 9 except that the ring's potential vorticity depths at the core and rim are approximately 1.7 and 0.9 (respectively) so that the core is not close to that of a zero potential vorticity ring.

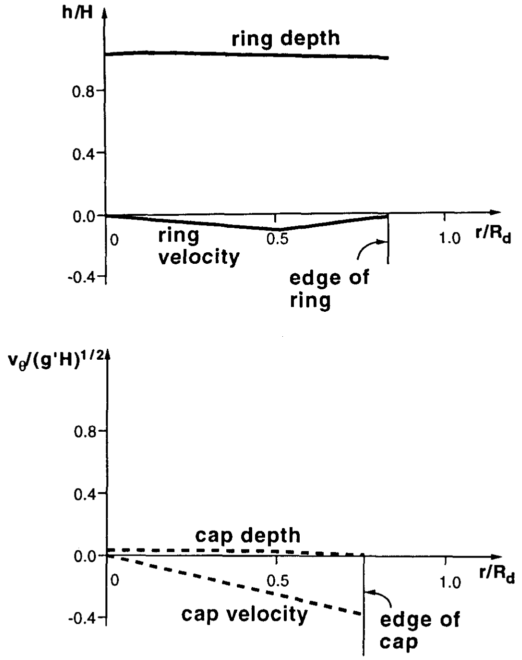

Fig. 13. The same as Fig. 10 except that the corresponding initial conditions are those shown in Fig. 12.

As expected, ringlets must be formed again in order to conserve angular momentum. As in the analytical case, the change in the system center of gravity is negligible; the energy loss associated with the interaction shown in Figs. 9–11 is 21% and for that shown in Figs. 12–14 is 67%. As briefly mentioned earlier, the ringlet's size in the numerical case can be much greater than that of the analytical solution. In both of our examples the ringlet's size is roughly 20% of the parent ring, much greater than the few percent obtained earlier in the analytical case. This larger size is in better agreement with the observations which, as mentioned, suggest a diameter that is about one-fourth of the parent ring size.

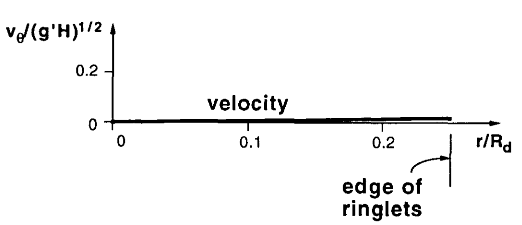

Fig. 14. As in Fig. 11 except that the corresponding initial conditions are those shown in Fig. 12.

4. Summary

Before listing our conclusions, it is perhaps appropriate to stress again the main elements of our models, the assumptions and the limitations of our study. Both the one-and-a-half-layer model (Fig. 5) and the two-and-a-half-layer model (Fig. 6) are nonlinear in the sense that both the Rossby number and the amplitude are of order unity. The transient interaction process was not directly addressed; instead, the initial and final states are connected assuming that the final state is steady. The main weakness of such an analysis is that, although the detailed structure of the final state is solved for, the general pattern of the final state is actually assumed. Hence, the validity of the result depends on the correctness of the assumed pattern. Nevertheless, the results are useful and may provide an explanation for the ringlets' formation process. Specifically, it is suggested that ringlets result from interactions of warm-core rings with waters lighter than their immediate surroundings. Such interactions (with, say, shelf water or the Gulf Stream) cause an entrainment of light water into the core of the ring which, due to conservation of angular momentum, causes, in turn, an expulsion of ring fluid. The entrainment takes place in such a manner that the entire ring is capped (Fig. 4). The associated expulsion of fluid from the rim must take place in terms of eddies formed via instabilities along the edge.

After the completion of this study the author became aware of Wang's (1992) recent study on ring-shelf water interactions. Using contour dynamics techniques he showed that, as a result of the ring-shelf water interaction, shelf water intrudes along the periphery of the ring. As expected from earlier studies on similar intrusions (e.g., Stern and Pratt 1985, Spitz and Nof 1991), the nose curls up and forms a cyclone. Such a mechanism provides an alternative explanation for the ringlets' expulsion process proposed here. As is frequently the case, however, the actual oceanic process is probably not as simple as either one of the proposed mechanisms. In reality, the actual generation process is probably some sort of combination of the two processes.

Two future examinations are suggested by our present analysis. From an observational point of view, it will be useful to determine whether the formation of ringlets is indeed correlated with prior interaction episodes. On the computation side, it would be useful to examine the entire time-dependent process so that the correctness of our final state can be examined.

5. Acknowledgements

Computations were made by Steve Van Gorder and the drawings by Beth Raynor. The study was supported by the Office of Naval Research grant number N00014-89-J-1606 and the National Science Foundation grants number OCE-9012114 and OCE-9102025.

Appendix A

List of symbols

AM	angular momentum
b	strip's distance from the ring
b^*	nondimensional distance between the ring's center and the strip
f	Coriolis parameter
g'	"reduced gravity," $(\Delta\rho/\rho)\, g$
H	undisturbed current depth at infinity $(x \to \infty)$
h	depth
h_c	depth of the cap
$\hat{h}$	depth at the ring's center $(r = 0)$
$\hat{h}_r$	ringlet's central depth
$\hat{h}^{(1)}$	nondimensional perturbation to the ring's original central depth $(\hat{h})^*$
$(\hat{h})^*$	nondimensional parent ring's depth
$(\hat{h}_r)^*$	nondimensional ringlet's central depth
$h_c^{(0)}$	zeroth-order approximation of the cap's depth
$h_c^{(1)}$	first order approximation of the cap's depth
h_c^*	nondimensional cap's depth
H_e	depth along the ring's edge
H_{p1}	potential vorticity depth of the core $(r \leqslant R_1)$
H_{p2}	potential vorticity depth of the rim $(R_1 \leqslant r \leqslant R_2)$
L	length of the strip
L^*	nondimensional length of the initial strip
N	number of ringlets
r, θ	polar coordinates
R_d	Rossby deformation radius, $(g'H)^{1/2}/f$
r^*	nondimensional radius
R_i^*	initial radius of the (parent) ring
u, v	velocities in Cartesian coordinates
$v_c^{(0)}$	zeroth-order approximation of the cap's orbital velocity
$v_c^{(1)}$	first order approximation of the cap's orbital velocity
v_θ	orbital velocity
v_θ^*	nondimensional orbital velocity
$v_{\theta c}$	orbital velocity of the cap
$v_{\theta c}^*$	nondimensional orbital velocity of the cap
$\bar{v}$	matched orbital speed along the front $(r = R_1)$
w	width of the strip
ΔE	energy loss
ε	ratio between the width of the strip which is later absorbed by the ring (w) and the deformation radius
μ	a small nondimensional parameter
ψ	streamfunction (defined by $\partial\psi/\partial y = -uh$; $\partial\psi/\partial x = vh$)

REFERENCES

Ball, F. K. 1963. Some general theorems concerning the finite motion of a shallow rotating liquid lying on a paraboloid. *J. Fluid Mech. 17*, 240–256.

Cushman-Roisin, B. 1989. On the role of filamentation in the merging of anticyclonic lenses. *J. Phys. Oceanogr. 19*, 253–258.

Evans, R., Baker, K., Brown, O. and Smith, R. 1985. Chronology of warm-core ring 82-B. *J. Geophys. Res. 90*, 8803–8811.

Kennelly, M. A., Evans, R. H. and Joyce, T. M. 1985. Small-scale cyclones on the periphery of a Gulf Stream warm-core ring. *J. Geophys. Res. 90*, 8845–8857.

Nof, D. 1990a. The breakup of dense filaments. *J. Phys. Oceanogr. 20*, 880–889.
Nof, D. 1990b. The role of angular momentum in the splitting of isolated eddies. *Tellus 42A*, 469–481.
Nof, D. 1991. Fission of single and multiple eddies. *J. Phys. Oceanogr. 21*, 40–52.
Paldor, N. and Nof, D. 1990. Linear instability of an anticyclonic vortex in a finite depth ocean. *J. Geophys. Res. 95*, 18,075–18,080.
Press, W. H., Flannery, B. P., Teukolsky, S. A. and Vetterling, W. T. 1986. *Numerical recipes: the art of scientific computing*. Cambridge University Press, 818 pp.
Spitz, Y. and Nof, D. 1991. Separation of boundary currents due to bottom topography. *Deep-Sea Res. 38*, 1–20.
Stern, M. and Pratt, L. 1985. Dynamics of vorticity fronts. *J. Fluid Mech. 161*, 513–532.
Wang, X. 1992. *Interaction of an eddy with a continental slope*. Massachusetts Institute of Technology and Woods Hole Oceanographic Institution Joint Program in Oceanography. Ph.D. thesis, 216 pp.